Electronic Supplementary Material (ESI) for Nanoscale.

A diffusive ink transport model for lipid dip-pen nanolithography

A. Urtizberea and M. Hirtz*

INKING PROCEDURE

Tip array of type F consists of 2 reading and 24 writing rectangular cantilevers with silicon nitride tips, with a tip-tip distance of 35 μm. F1-2 inkwell chips include twelve reservoirs that drive the ink to twelve microfluidic channels separated each by 70 μm, therefore matching up either with the even or the odd writing tips of the tip array. Each micron-size ink reservoir of the chip was loaded by using a pipette with 1 μL of the phospholipid ink solution DOPC 20 mg/mL (25.4 mM) doped with 1 mol% of Liss Rhod PE. The chloroform solvent was allowed to evaporate in the inkwells for 40 min in a vacuum desiccator before coating the tips.

The tips were then coated by placing them into contact with the inkwells for 2 min at 70% relative humidity, coating all even tips.

After inking, excess ink was wiped off by writing on a sacrificial area on the sample, so the tips are freed from excessive ink before performing the actual intended lithographic structure.

TIP-SURFACE APPROACH

There are two general procedures to approach the tip array near to the surface prior to patterning.

The first method relies on purely optical alignment. Here, the tip array is first carefully focused in the in-built optical microscope of the system and the Z-scanner is set to maximum extension (8.8 μm). Then the Z-stage is lowered in small steps until the cantilever deflect on contact with the surface, which leads to a color change of the light reflected from the cantilevers. Prior to writing, the Z-stage is then lifted again by 12 μm. Though the optical microscope can detect bending of a tip once the z position is moved 5 μm beyond the point of contact with the surface,[1] the final step of raising the Z-stage piezo about 12 μm is actually accounting for the visual errors detecting the surface and the stage positioning hysteresis.

The second, much more precise, method employs the laser alignment and surface approach usually employed in AFM. One of the reader tips is taken as reference for approach and the laser spot of the AFM feedback system is positioned on the end of this cantilever. Then the photodetector is adjusted until the signal lies within the 'contact mode' region. Then the Z-scanner piezo (fine movement piezo) is extended 8.8 μm down towards the surface. Starting with the tip array 100 μm away from the substrate surface, the Z-stage piezo is then lowered in small steps towards the surface while monitoring the photodetector signal, till a signal change in the photodetector shows. Then the Z-scanner piezo extension is lowered, until a specified change in signal compared to the 100 μm reference is reached, the specific value being calibrated as described below in the next paragraph. The determined extension of the Z-scanner piezo is then used in the lithography setting as extension for pattern writing (Z-piezo extension).

In order to determine the Z-piezo extension needed for a reproducible surface approach and a stable patterning following experiments were conducted: First a specific tip surface distance was set by a fixed value of the Z-stage piezo upon surface detection, and then lithography was performed with different values for the Z-scanner piezo extension. Interestingly, these experiments showed that no stable patterning is seen at any of the humidities employed here when the value of the Z-piezo extension during lithography is exactly set to the value of the Z-scanner piezo as the surface is just detected, i.e. when the signal on the sensor diode is just starting to change to less negative values. The value required of Z Piezo Extend to stable pattern corresponds (Z-scanner piezo has a distance/voltage constant of 0.07 μm/V) to an additional surface-tip approach of approximately 0.5 μm.

As already mentioned, the photodetector is adjusted far away from surface until the signal lies within the 'contact mode' region (meaning negative sensor voltage). Starting from this voltage, as the surface is first detected the detected voltage value initially moves towards more negative values, indicating that the tip is pulled closer to the surface. This takes place along a Z-scanner piezo travelling distance of about 1 μm. Using exactly this value for Z-piezo extension during lithography does not provide any patterning, at any of the working humidities. Then as the Z-scanner piezo is further approached to the surface the sensor voltage starts growing again, yielding less negative values, thus indicating that the tip is now pushed

away from the surface. Using an extension corresponding to this value to set the Z-piezo extension during lithography allows patterning, although for a stable patterning the additional 0.5 μm approach is mandatory. We can tentatively assign this feature of an attractive and repulsive regime to the creation of a meniscus between surface and tip pulling it towards the substrate before the repulsive regime interaction with the surface sets in.[2,3] The length of the initial pulling regime depends on the substrate: for Au substrates it is around 3 μm. For OTS treated surfaces this regime is not observed, indicating that substrate hydrophobicity influences the meniscus formed and thus the associated capillary-bridge force.

Right after the repulsive regime starts, approaching additional 5 μm towards the surface leads to the loss of laser deflection. The piezo has yet to travel additionally 5 μm towards surface to see the cantilever deflection in the microscope, as in the 'optical' surface approach procedure. This makes about 10 μm from the surface detection which is, within some error due to piezo non-linearities and 'eye detection', the distance the Z-stage piezo is usually raised upon surface detection following the 'visual' surface approach.

It should be noted that one common element of all contact-mode pens is that the cantilever has a very low spring constant (*k*, the spring constant, is as low as 0.097 nN/nm). This is ideal for surface detection while monitoring the sensor voltage change, since the pen quickly bends while sensing the surface topography without gouging the surface. An overly stiff cantilever would damage the surface by scratching the softer substrate. This surface approach has been used for patterning over substrates as soft as 10 nm Au thin films (results not shown here) in which no damage of the surface is seen in AFM and dark field microscopy.

STRUCTURAL CHARACTERIZATION

The area obtained by fluorescent microscopy shows larger standard deviations than the one determined by AFM, as shown in Fig. S1. Additionally, when features within a very different size scale range are compared, larger ones show an increased deviation from the value measured with the AFM. This feature may arise from the proximity effect leading to extra illumination that also accounts for the reported shape-dependent behavior for fluorescence intensity as proposed in ref. 4.

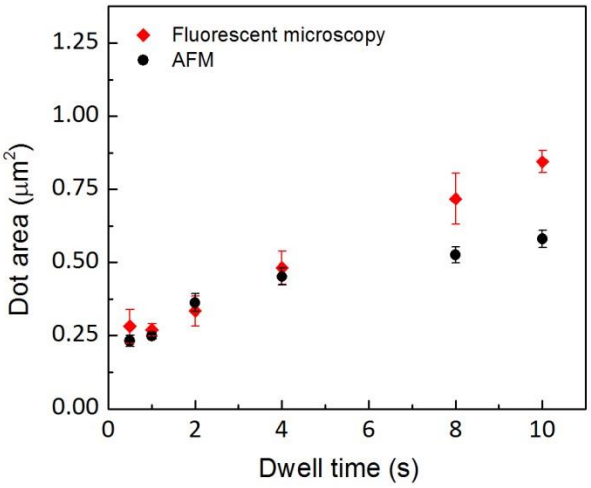

Fig. S1 Area of DOPC dots patterned on glass at RH 32.8 ± 0.2% measured by Fluorescent microscopy (◆) and AFM (●) . Bars represent the error of four samples average.

Additionally, while it was reported that fluorescent microscopy can be applied for thicker structures, on thin ones within the order of only a few bilayers (below 10 nm), self-quenching and phase separation can become an issue and the admixing of the fluorescent probe itself might introduce an unwanted additional component to the ink.[5] For the present study, we therefore relied on the generally more reliable AFM data.

One aspect to be consider when such small L-DPN features are scanned with AFM is that they are prone to shape changes at low scan speeds, as shown in Fig. S2. This can be attributed to water condensation between tip and lipid structure that may allow the feature to rearrange. It should be noted, that shapes as shown in Fig. S2(a) are unusual in L-DPN dot patterns, as usually circular shaped domes are found, in which this change of shape after AFM scanning is not so

clearly evident (usual features look like Fig. 2(b)). Speed tests (data not presented here) showed that keeping speed above 15 μm/s avoids features distortion.

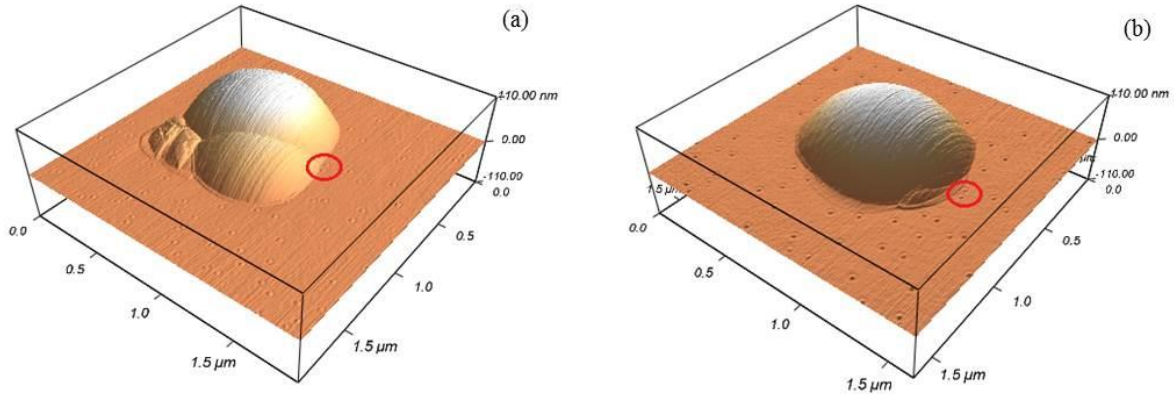

Fig. S2 3D AFM images of a dot patterned on glass at RH 34.5 ± 0.2% measured at 0.9 μm/s. (b) Was measured two days after (a). Note red circles are a guide of the marks over the substrate that show same sample has been scanned.

As the speed should be kept above 15 μm/s, and in order to keep a good resolution of the structural data, samples were scanned first in a large scan (4 rows x 3 dwell times), and then zooming in for a smaller scan of one of the four dots for each dwell time, at each RH. As shown in Fig. S3 for RH 37.8 ± 0.1%, average of four samples is in very good agreement with the scan of a single dot, thereby indicating the accuracy of the reported structural data.

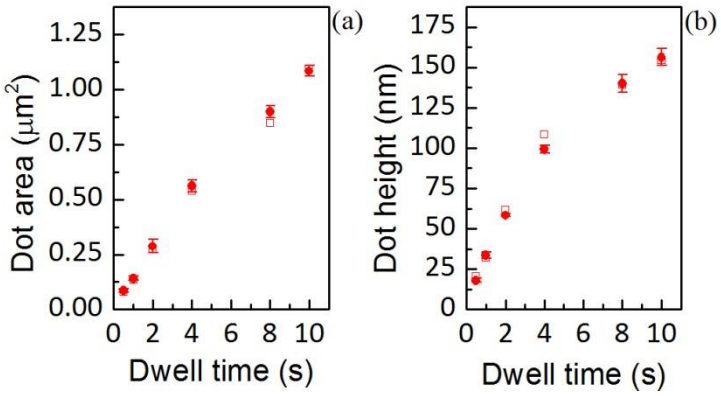

Fig. S3 Area of DOPC dots patterned on glass at RH 37.8 ± 0.1% measured by AFM. (●) represent four samples average; (□) is the scan of one dot.

AREA AND HEIGHT GROWTH

The area and height growth is shown in Fig. S4.

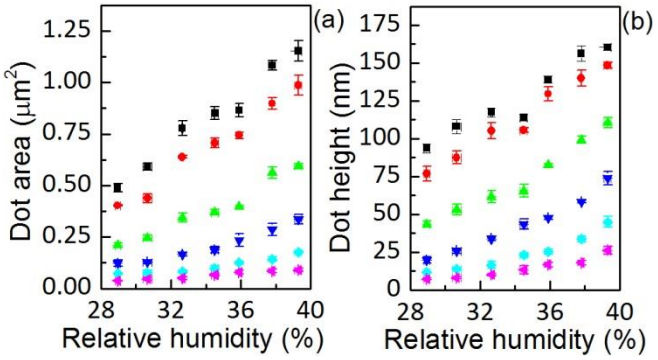

Fig. S4 Surface spread and height dependence with humidity at dwell times 10 s (■), 8 s (●), 4 s (▲), 2 s (▼), 1 s (◆), and 0.5 s (◀).

TIPS COMPARISON: AREA, FLOW RATE AND WETTING ANGLE

The ink transport mechanism corresponding to four tips of the same tip array have been analyzed. This is shown in Fig. S5. They are named as tip 1, tip 4, tip 6, and tip 9. Taking tip 1 as the reference, tip 4 is at 280 μm, tip 6 is at 420 μm, and tip 9 is at 700 μm distance from the tip1 in the tip array.

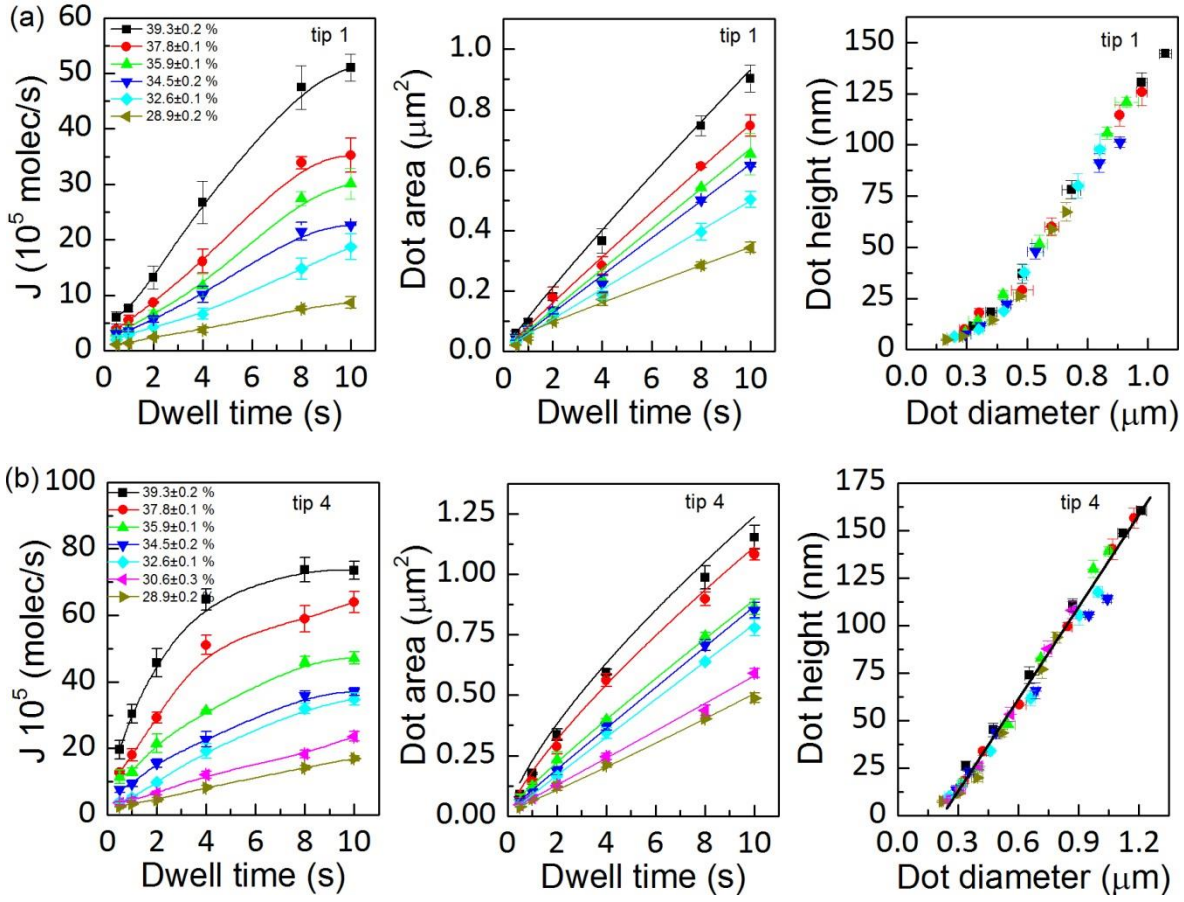

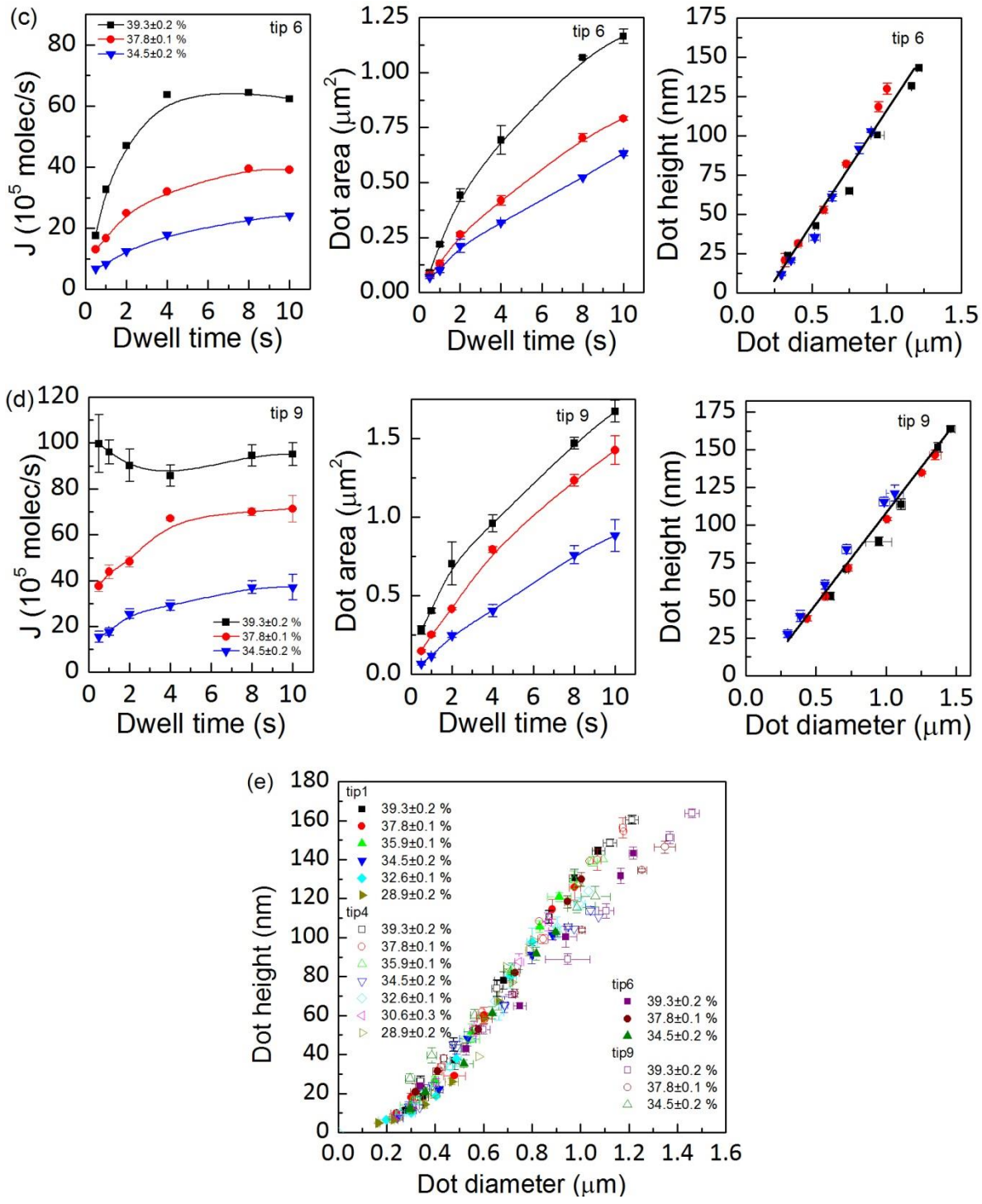

Fig. S5 Flow rate, surface spreading and height versus diameter (h /w = (1/2) tan(θ/2)) for four tips at different humidities. Taking tip 1 as the reference, tip 4 is at 280 μm, tip 6 is at 420 μm, and tip 9 is at 700 μm distance from tip 1. Note that the flow dynamics and surface spreading are correlated: at higher flow J(t) becomes saturated earlier and S(t) departs from S(t) α t. The height vs distance for four tips at different humidities shows that contact angle is in agreement for all the four tips at any humidity. Notice that for tip 1, at very small sizes, the wetting angle becomes dependent of the size, maybe due to the dependence of the line tension with the contact angle at small sizes.

It should be noted that not only the ink flow, but the flow rate itself (dynamics) changes, thereby it is advisable in order to get a comprehensive picture of the ink transport, to analyze only one tip at a time within varying experimental conditions. As discussed in the main article, this is mainly due to the dynamic dependence of the flow itself, which is not just a simple proportionality factor.

Relevant information concerning flow rate and surface spreading can be deduced by comparing the flow rate and spreading dynamics within the tips in the tip array in Fig. S5. There is a tendency of the spreading and flow rate visible as the tip is further away from the reference tip. Mainly, the flow increases, getting J(t) saturated faster and S(t) diverts from the linear S(t) α t behavior. As discussed in the main article, this correlation between the saturation of the flow rate (J(t) dynamics) and the surface spreading dynamics, shows that both magnitudes are correlated: J(t) governs S(t), yet J(t) is affected by differences in concentration at the meniscus/surface (Fickian flow).

Despite this correlation, when different tips of the same tip array are compared, the wetting angle of the tips is in agreement at different RH, as shown in Fig. S5(e). This indicates that surface energy governs the final shape of the feature. It is interesting to note that at very small sizes, as attained by tip 1, this linearity ceases, but extrapolation yields a well-defined intersection value of about 200 nm. Yet, since line tension stems from the molecular interactions between the three phases at the vicinity of the contact line, at very small sizes it is no longer independent of the contact angle, thereby breaking the h/d proportionality rule, and making the contact angle to become size dependent.[6,7]

TIP SIZE AND WEAR

The tips were measured by SEM in order to get an estimation of the average tip size and compare it with the estimated meniscus of about 200 nm.

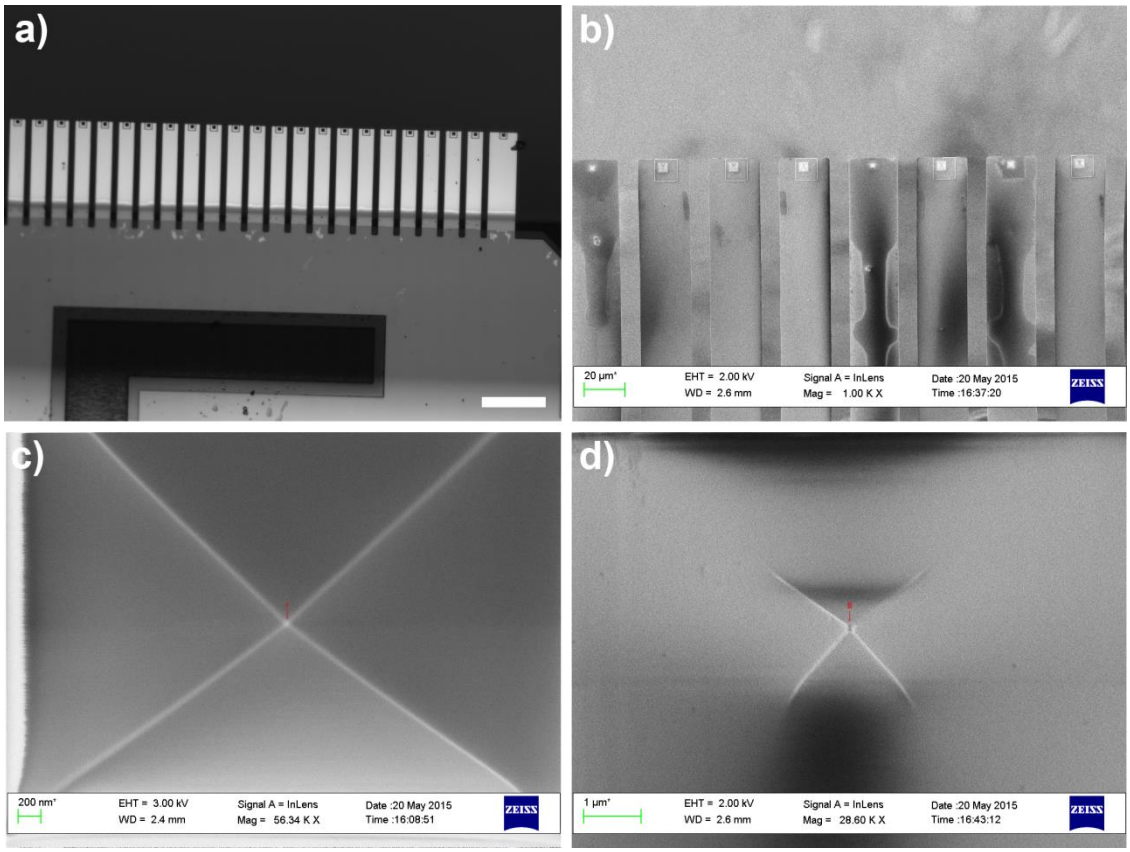

Fig. S6 a) Usual F type tip array; b) Tip array after the patterning. The tip analyzed in the main text corresponds to the fifth tip of image b); c) Tip of an unused tip array with marked area 23 x 31 nm²; d) tip analyzed in the main article with marked area 74 x 111 nm², where long distance may correspond to image distortion as noticed in the image.

The tips are non-conductive and we did not want to alter the tip apex by coating of conductive materials, thereby the images show distortions stemming from charging effects, especially in case of the used tips, that additionally carry a layer of lipid ink over the tip and cantilever. Nevertheless, images allow an estimation of the area of 23 x 31 nm² (new tip) and about 74 x 111 nm² (after lithography), respectively.

FIT ALLOWING TIME DEPENDENCE OF D_0c_0

The fit of the experimental data for dot feature area versus dwell time with Eq. (11), shown in Fig. 14 of the main article, can be improved letting D_0c_0 increase with the time as $D_0c_0\,(t) = D_0c_0\,(0) + D^*[1\text{-}\exp(-\alpha t)]$. Yet this function introduces two additional parameters into the fit. This dependence points to a possible progressive hydration mechanism of the lipids at the tip/meniscus, in agreement with the qualitative picture of the ink supply drawn in Sec. 3.1.

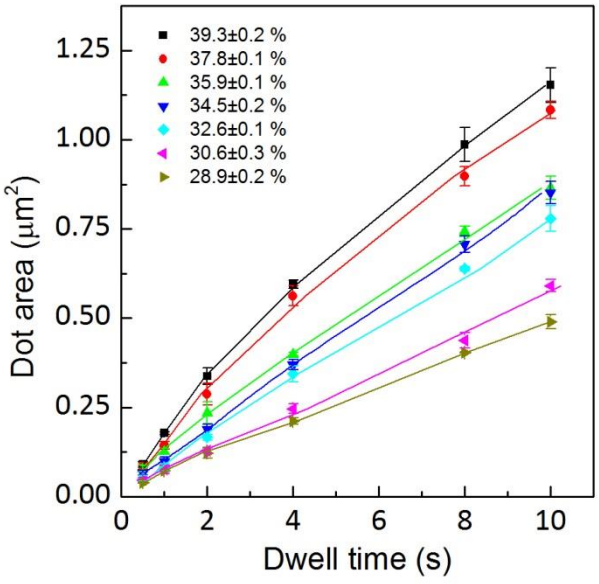

Fig. S7 Fit of the dot feature area versus dwell time with Eq. (11), allowing $D_0c_0\,(t) = D_0c_0\,(0) + D^*[1\text{-}\exp(-\alpha t)]$.

1 K. Salaita, S. W. Lee, X. Wang, L. Huang, T. M. Dellinger, C. Liu and C. A. Mirkin, *Small*, 2005, **1**, 940–945.

2 P. A. Kralchevsky and K. Nagayama, in *Particles at Fluid Interfaces and Membranes*, Amsterdam, Elsevier., 2001, pp. 469–502.

3 J. Crassous, E. Charlaix and J.-L. Loubet, *Phys. Rev. Lett.*, 1997, **78**, 2425–2428.

4 O. A. Nafday and S. Lenhert, *Nanotechnology*, 2011, **22**, 225301.

5 M. Hirtz, R. Corso, S. Sekula-Neuner and H. Fuchs, *Langmuir*, 2011, **27**, 11605–11608.

6 D. Li, in *Colloids and Surfaces A: Physicochemical and Engineering Aspects*, 1996, vol. 116, pp. 1–23.

7 A. Marmur, *J. Colloid Interface Sci.*, 1997, **186**, 462–6.